**Bulletin of Electrical Engineering and Informatics**
Vol. 11, No. 3, June 2022, pp. 1317~1324
ISSN: 2302-9285, DOI: 10.11591/eei.v11i3.3766 

# Two-layer remote phosphor package as a solution to promote color quality scale and lumen in WLEDs

**Phuc Dang Huu[1], Dieu An Nguyen Thi[2]**
[1]Institute of Applied Technology, Thu Dau Mot University, Binh Duong, Vietnam
[2]Faculty of Electrical Engineering Technology, Industrial University of Ho Chi Minh City, Hồ Chí Minh, Vietnam

**Article Info**

***Article history:***

Received Jun 9, 2021
Revised Jan 20, 2022
Accepted Apr 16, 2022

***Keywords:***

Color rendering index
$LaAsO_4:Eu^{3+}$
Mie-scattering theory
Two-layer phosphor
WLEDs

**ABSTRACT**

This article demonstrates the influence of the red-light $LaAsO_4:Eu^{3+}$ phosphorus on the optical features of the two structures: one-layer remote phosphorus scheme (SRPS) and two-layer remote phosphorus scheme (DRPS). As a result, the Mie hypothesis is used to demonstrate and prove the comparison between color quality and luminosity (LF) between these two factors. The SRPS is a phosphor layer that consists of $LaAsO_4:Eu^{3+}$ particles combined with the $YAG:Ce^{3+}$ mixture. Meanwhile, DRPS is two phosphor layers of red and yellow separated from each other. To improve the dispersing property, 5% of $SiO_2$ is combined with the phosphorous films. The difference between the structures influences the optical features of WLEDs. The obtained outcomes show that the color rendering index (CRI) rises along with the concentrations of both structures while these values are nearly identical to each other. Meanwhile, at ACCTs (5600 K - 8500 K), the color quality scale (CQS) in DRPS reaches 74, which is higher than SRPS's 71 at 8500 K. Besides, the lumen in DRPS is considerably greater than that in SRPS at 2%-14% $LaAsO_4:Eu^{3+}$. In short, DRPS brings considerable benefits to the color quality and lumen when compared to SRPS. In addition, choosing a suitable concentration also becomes highly vital to achieve desirable CQS and LF.



***Corresponding Author:***

Dieu An Nguyen Thi
Faculty of Electrical Engineering Technology, Industrial University of Ho Chi Minh City
No. 12 Nguyen Van Bao Street, Ho Chi Minh, Vietnam
Email: nguyenthidieuan@iuh.edu.vn

## 1. INTRODUCTION

White light-emitting diodes (abbreviated as WLEDs) offer many benefits such as significant lumen performance, significant energy performance, insignificant volume while posing no harm to the environment, and as such can become a promising substitute for traditional incandescent and fluorescent light [1]. Usually, it takes blue color chips with the yellow $Y_3Al_5O_{12}:Ce^{3+}$ (YAG:Ce) phosphorus to create phosphor-converted (pc)-WLEDs [2]. However, because of the red-light elements limited amount, such a technique can result in a lower color rendering indice (CRI) and significant correlated color temperature (CCT) [3]. In order to create certain pc-WLEDs, we can integrate a near-ultraviolet (UV) chip featuring multi-color phosphors. Such procedure is intended to yield a greater CRI compared to that in pc-WLEDs based on YAG:Ce. By combining the near-UV light-emitting diodes (LEDs) with suitable phosphors, we can obtain a wide spectrum, great CRI results, and will be able to adjust the CCT value [4]. Silicate phosphors possess a strong near-UV absorption property as well as a great quantum efficacy. Researches have examined the silicate phosphors that generate blue and green light ($BaZrSi_3O_9:Eu^{2+}$ [5], [6] and $Ba_2MgSi_2O_7:Eu^{2+}$ [7], [8], respectively) and employed them in near-UV LEDs. Furthermore, red $Ca_2Si_5N_8:Eu^{2+}$ phosphors were also made at standard pressure using the solid-state reaction approach [9]. For the current effort, near-UV chips of LED carry the task of pumping triple-chroma phosphors to create pc-WLEDs that yield considerable CRI values. The contents of the layers of phosphor include 5-wt% red $Ca_{1.97}Si_5N_8:0.03Eu^{2+}$ phosphor and 95-wt% silicone gel. Layers of mixed phosphors are made of 10-wt% blue $Ba_{0.5}Sr_{0.4}ZrSi_3O_9:0.1Eu^{2+}$ phosphor and 15-wt% green $Ba_{1.94}MgSi_2O_7:0.06Eu^{2+}$.

In order to create traditional pc-WLEDs, several phosphors are mixed with gels used to paint the chips of LED, and as a result, this will lower the pc-WLEDs' effectiveness and chromatic genuineness, caused by the incomplete re-absorption among the phosphors with an overlay of the spectrum [10]. A structure with layers separated, with a red layer of phosphor placed beneath the yellow layer, has shown the ability to impede the impact of re-absorption [9], [11], [12]. As far we are concerned, there have been no studies before that use divided layers in triple-phosphor WLEDs. Because of the three divided phosphors, adjusting the covering parameters becomes exceedingly difficult for the task of creating big-CRI WLEDs. We cannot easily detect the re-absorption event happening among the blue and green phosphors. As such, our research makes alterations to the said structure with a layer of red phosphor (R) placed beneath a mixed-phosphor layer of blue and green (B&G) to create pc-WLEDs that can yield great CRI values. The research also assesses the impact of the overlaying zone among the deconvoluted peaks from the pc-WLEDs' electroluminescence (EL) on the CRI results. The pc-WLEDs recommended yield considerable CRI results and a CCT that we can modify by changing the phosphor layer's thickness. The features of the recommended apparatuses are compared to ones mentioned in published works [13], [14]. Besides the benefits of illumination efficiency and the thermal stability of the WLEDs, PiG also benefits the color quality, which has been clearly mentioned or proven in very few researches. The optical properties of WLEDs, such as illumination efficacy and colour fidelity, are optimized in this study employing a new two-layer distant phosphorus scheme (DRPS). Furthermore, the Mie-scattering hypothesis convincingly proves the optical feature distinction of the two structures of one-layer remote phosphorus scheme (SRPS) and DRPS.

## 2. EXPERIMENT AND SIMULATION DETAILS

### 2.1. The simulation process of SRPS and DRPS

To reconstruct the WLED models at the following average CCT values, we used the commercial tool lighttools 9.0, which is developed using the monte carlo ray-tracing approach. Figure 1(a) shows the remote phosphor package with temperatures of 8500 K, 7700 K, 7000 K, 6000 K, and 5600 K. The real-life WLED 3D-recreation model intended to optically simulate the remote phosphor package (Figure 1(b)). SRPS is a phosphor layer consisting of $LaAsO_4:Eu^{3+}$ particles combined with the $YAG:Ce^{3+}$ mixture as seen in Figure 1(c). Meanwhile, DRPS is two phosphor layers of red and yellow separated as seen in Figure 1(d).

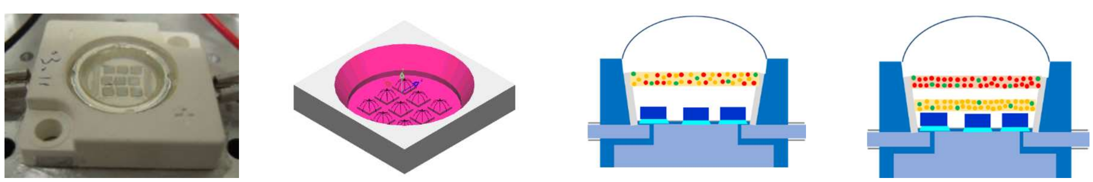

(a) (b) (c) (d)

Figure 1. Schematic diagrams of phosphor-converted WLEDs, (a) WLEDs demonstration, (b) WLEDs model utilizing LightTools approach, (c) demonstration of SRPS featuring $SiO_2$ (green) and $LaAsO_4:Eu^{3+}$ (red) in $YAG:Ce^{3+}$ compound (yellow), and (d) demonstration of DRPS featuring $SiO_2$ in $LaAsO_4:Eu^{3+}$ compound $YAG:Ce^{3+}$ compound

For the real-life WLED model, the reflector's bottom area, height, and peak-surface area are respectively 8-mm, 2.07-mm, and 9.85-mm. The remote phosphorus film is 0.08-mm thick by default and conceals the nine chips of LED. All square chips are 1.14 mm long, 0.15 mm tall and are attached to the reflector's gap, which we can see in Figure 1(b). At 455 nm wavelength, the chips exhibit a 1.16 W radiant flux. At 5% $SiO_2$ particle concentration in the phosphorus composition, $LaAsO_4:Eu^{3+}$ phosphorus concentration particle shifts constantly from 2% to 30%. Nevertheless, we can manipulate $YAG:Ce^{3+}$ wt to keep the CCTs at an average level. We use the LightTools 9.0 application to recreate the optical features of the $SiO_2$ and $LaAsO_4:Eu^{3+}$ phosphor motes. For the $SiO_2$ and $LaAsO_4:Eu^{3+}$ phosphors, their nonmandatory refractive indexes of the diffuses have responding values of 1.54 and 1.08. The spherical $SiO_2$ motes have an average 3-µm radius when mie-simulated. On the other hand, the phosphor motes attain a 7.25 µm median radius and a 1.83 refractive indice, regardless of the optical wavelengths with the silicone adhesive's 1.5 refractive indice. The diffusive particle density stands out to sustain the average CCT level. To sustain the CCT in case the diffuses' weight percentage rises, we must lower the YAG:$Ce^{3+}$ phosphor's weight.

## 2.2. Preparation of $LaAsO_4$:$Eu^{3+}$ phosphor

The preparation process begins with mixing the listed ingredients by dissolving them in $H_2O_2$ of 30%. Then, continuing stirring slowly, heat the mixture until the boiling reveals the synthesis of $H_3AsO_4$. [15], [16]. The obtained composition is let to dry in the air, thereafter pulverized, see Table 1. The mixture then undergoes two firing phases. In the first phase, heat the mixture in air opened quartz boats at about 500°C, then pulverized. In the second phase, the same procedures are conducted but at the heat of 1000°C for an hour. The phosphor acquired emits red light, with emission peaks from 1.785–2.149 eV and excited efficacy by UV of +(91.88 eV), –(3.40 eV).

Table 1. Chemical composition of green-emitting phosphor $LaAsO_4$:$Eu^{3+}$

| Ingredient | Mole % | By weight (g) |
|---|---|---|
| $La_2O_3$ | 95 (of La) | 155 |
| $Eu_2O_3$ | 5 (of Eu) | 8.8 |
| $As_2O_3$ | 100 (of As) | 75 |

## 3. SCATTERING COMPUTATION

Based on the theory of Mie-scattering [17]-[23], the three formulas below are used to calculate the scattered coefficients $\mu_{sca}(\lambda)$, anisotropy element $g(\lambda)$, and decreased scattered coefficients $\delta_{sca}(\lambda)$:

$$\mu_{sca}(\lambda) = \int N(r) C_{sca}(\lambda, r) dr \quad (1)$$

$$g(\lambda) = 2\pi \int \int_{-1}^{1} p(\theta, \lambda, r) f(r) cos\theta dcos\theta dr \quad (2)$$

$$\delta_{sca} = \mu_{sca}(1 - g) \quad (3)$$

For the formulas demonstrated, the N(r) symbol represents diffusional particles' density of allocation (measured in $mm^3$), the $C_{sca}$ symbol represents the scattered cross-section in $mm^2$, the $p(\theta,\lambda,r)$ symbol represents the phase role, the λ symbol represents the optical wavelengths in nm, the r symbol represents diffusive particles' radius in µm, the θ symbol represents the scattered angle in °C, and the f(r) symbol represents the diffusor size distributing role within the phosphorus film, as seen in the formulas:

$$f(r) = f_{dif}(r) + f_{phos}(r) \quad (4)$$

$$N(r) = N_{dif}(r) + N_{phos}(r) = K_N.[f_{dif}(r) + f_{phos}(r)] \quad (5)$$

The N(r) value includes the diffusional ions' density and the phosphor particle's intensity, respectively indicated by the symbols $N_{dif}(r)$ and $N_{phos}(r)$. The symbols $f_{dif}(r)$ and $f_{phos}(r)$ represents the diffusor's and the phosphor mote's size distribution function data respectively. The $K_N$ symbol represents the amount of diffusor unit for each concentration of the diffusor, which is determined by the following formula:

$$c = K_N \int M(r) dr \quad (6)$$

The following equation determines $M(r)$, which is the diffusive unit's gross allocation:

$$M(r) = \frac{4}{3}\pi r^3 [\rho_{dif} f_{dif}(r) + \rho_{phos} f_{phos}(r)] \quad (7)$$

In (7), the symbols $\rho_{diff}(r)$ and $\rho_{phos}(r)$ represent diffusor's and phosphor crystal's density. Derived from the Mie-scattering hypothesis, the following formula determines $C_{sca}$:

$$C_{sca} = \frac{2\pi}{k^2} \sum_0^{\infty} (2n - 1)(|a_n|^2 + |b_n|^2) \quad (8)$$

With $k=2\pi/\lambda$ (9) and (10) determines $a_n$ and $b_n$:

$$a_n(x,m) = \frac{\Psi'_n(mx)\Psi_n(x) - m\Psi_n(mx)\Psi'_n(x)}{\Psi'_n(mx)\xi_n(x) - m\Psi_n(mx)\xi'_n(x)} \quad (9)$$

$$b_n(x,m) = \frac{m\Psi'_n(mx)\Psi_n(x) - \Psi_n(mx)\Psi'_n(x)}{m\Psi'_n(mx)\xi_n(x) - \Psi_n(mx)\xi'_n(x)} \quad (10)$$

Where *x*=*k.r*, *m* indicates the refractive indice, $\Psi_n(x)$ along with $\xi_n(x)$ indicating the Riccati-Bessel role.

Figure 2 demonstrates that the scattered coefficients are directly proportional to the phosphor $LaAsO_4:Eu^{3+}$ concentration. For the $LaAsO_4:Eu^{3+}$ and $SiO_2$ particles, their scattering events have a remarkable impact on the RP-WLEDs. Compared to the LED's blue light, the $LaAsO_4:Eu^{3+}$ phosphor possesses greater absorption property. Therefore, with the prevalence of the red light generated, we can supplement the red element in the RP-WLEDs. In addition, the 5% wt. concentration of $SiO_2$ that is intended to encourage the scattering property can improve the pc-LED's absorption property as well. As such, the granules of $LaAsO_4:Eu^{3+}$ and $SiO_2$ are intended to raise the chromatic performance of WLEDs. As we can see in Figure 3, the anisotropy aspect of $LaAsO_4:Eu^{3+}$ granules at the wavelength value range of 453 nm, 555 nm, 680 nm shows that the anisotropy aspect at 680 nm has greater values than that at 555 nm. Furthermore, compared to the remaining wavelengths, we can achieve the greatest values of the anisotropy aspect at the wavelengths of 453 nm. In other words, the $LaAsO_4:Eu^{3+}$ granules can improve the chromatic homogeneity in RP-WLEDs. For the two structures of SRPS and DRPS, their silicone's refractive index ($n_{sil}$) has a value of 1.53. The $n_{phos}$ symbol indicates the phosphor granules' refractive index. As such, the diffusors and the phosphor's relative refractive indices in the silicone (indicated by $m_{dif}$ and $m_{dif}$ respectively) could be determined using $m_{dif} = n_{dif}/n_{sil}$ as well as $m_{phos} = n_{phos}/n_{sil}$. The phase role is subsequently determined by:

$$p(\theta,\lambda,r) = \frac{4\pi\beta(\theta,\lambda,r)}{k^2 C_{sca}(\lambda,r)} \quad (11)$$

The symbols $\beta(\theta,\lambda,r)$, $S_1(\theta)$ and $S_2(\theta)$, which indicates angular scattered amplitudes, are determined by the formulas [24]-[26]:

$$\beta(\theta,\lambda,r) = \frac{1}{2}[|S_1(\theta)|^2 + |S_2(\theta)|^2] \quad (12)$$

$$S_1 = \sum_{n=1}^{\infty} \frac{2n+1}{n(n+1)}[a_n(x,m)\pi_n(\cos\theta) + b_n(x,m)\tau_n(\cos\theta)] \quad (13)$$

$$S_2 = \sum_{n=1}^{\infty} \frac{2n+1}{n(n+1)}[a_n(x,m)\tau_n(\cos\theta) + b_n(x,m)\pi_n(\cos\theta)] \quad (14)$$

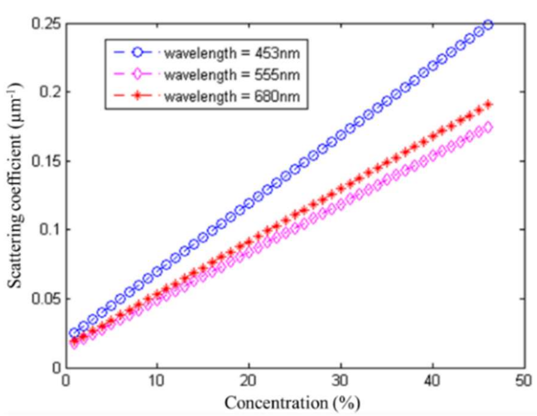


Figure 2. $LaAsO_4:Eu^{3+}$ scattered coefficients at 453nm, 555nm, and 680nm in wavelength values

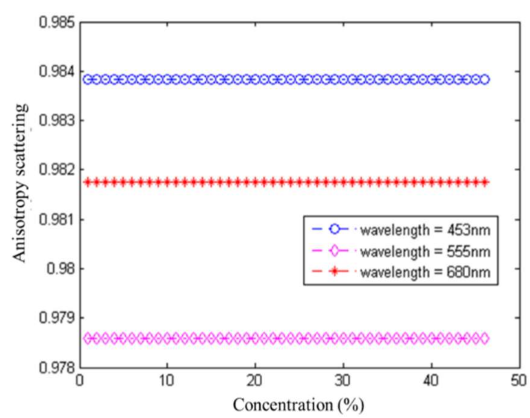


Figure 3. $LaAsO_4:Eu^{3+}$ anisotropy scattered process at 453nm, 555nm, and 680nm in wavelength values

## 4. RESULTS AND DISCUSSION

The approximate decreased scattering coefficient of $LaAsO_4:Eu^{3+}$ is directly proportional to the wavelength range from 453 nm, 555 nm, 680 nm, as seen in Figure 4. The consistency of scattering in $LaAsO_4:Eu^{3+}$ phosphor can be beneficial to the RP-WLEDs' chromatic performance. We then evaluate the angular scattering amplitudes of the $LaAsO_4:Eu^{3+}$ phosphor using the MATLAB application. According to the outcomes, the $LaAsO_4:Eu^{3+}$ phosphor granules greatly benefit the scattering of blue light. As more blue light is generated, the yellow-ring event will be decreased. In accordance with this, in Figure 5, the said granules can supplement the red light as well as the blue light. The main goal of such computations is to verify the outcomes shown from Figure 6 to Figure 8.

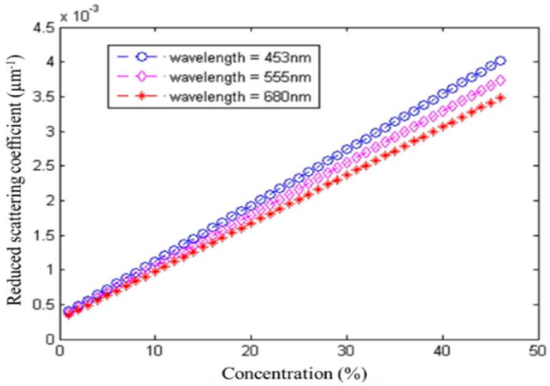


Figure 4. $LaAsO_4:Eu^{3+}$ decreased scattered coefficients at 453nm, 555nm and 680nm in wavelength values

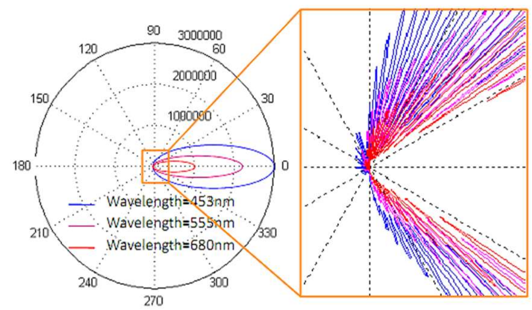


Figure 5. $LaAsO_4:Eu^{3+}$ the angular scattered amplitudes at 453nm, 555nm and 680nm wavelength values

The CRI value differences between the two structures of SRPS and DRPS is insignificant. As the concentration of $LaAsO_4:Eu^{3+}$ reaches 22%, the CRI of SRPS and DRPS show an upward trend. Notably, the CRI is directly proportional to the ACCT and is highest at 8500 K. This is a vital result that will contribute to the CRI improvement in both configurations. The phosphorus $LaAsO_4:Eu^{3+}$ can control the CRI at such great ACCT of 8500K. However, the CRI is a factor among the parameters intended to assess the colour standard. Recently, the color quality scale (CQS) has been the researching focus of various studies. CQS is the amalgamation of the three aspects: CRI, beholder's inclination as well as color coordination. By covering these three aspects, CQS becomes a significant target and "seemingly" the most important parameter applied to assess the colour standard. As the concentration of $LaAsO_4:Eu^{3+}$ surpasses 30%, the SRPS's CRI keep on growing. Meanwhile, the DRPS's CRI displays an downward trend at all ACCTs. This phenomenon also happens similarly to the CQS result in Figure 7. For the SRPS structure, the highest CQS value at 8500 K is 71. Meanwhile, the DRPS's CQS at mostly all ACCTs is reported 74. Therefore, DRPS yields better color quality than SRPS.

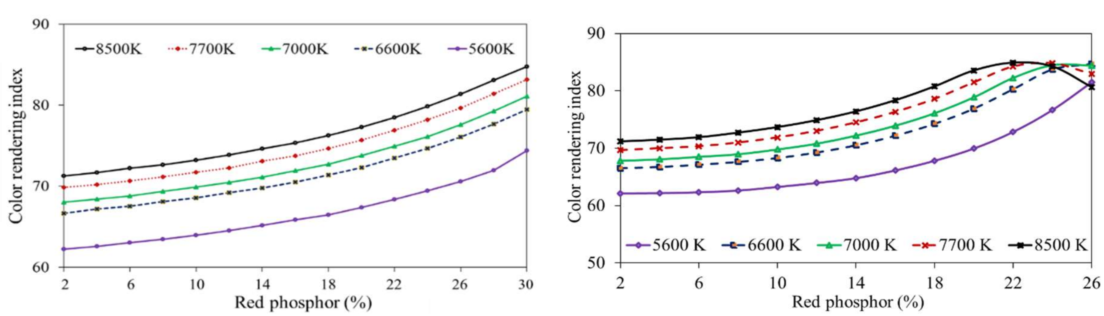


(a) (b)

Figure 6. CRI increase featuring $LaAsO_4:Eu^{3+}$ concentration (a) SRPS and (b) DRPS

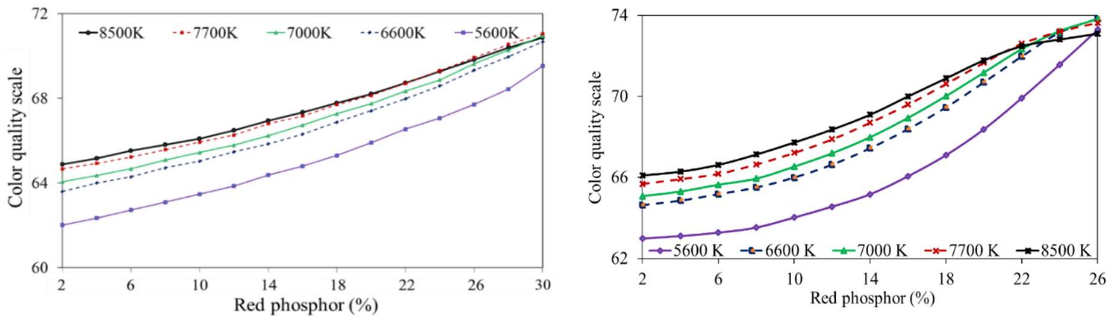


(a) (b)

Figure 7. CQS increase featuring $LaAsO_4:Eu^{3+}$ concentration (a) SRPS and (b) DRPS

The CRI and CQS values display a noticeable upward trend as the red phosphor concentration changes from 2% to 30% in Figures 6(a) to (b) and Figures 7(a) to (b). The CRI and CQS peak at 85 and 71 accordingly, at 30% $LaAsO_4:Eu^{3+}$ concentration. Furthermore, according to Figure 5, at the wavelength of 453 nm, the angular scattering amplitudes reach their peak, compared to those at the wavelengths of 555 nm or 680 nm. This indicates that the additional concentration of $LaAsO_4:Eu^{3+}$ can considerable positive effect on the scattering event of blue light, which can both boost the chromatic performance and the lumen. But in the SRPS structure, the phenomenon of backscattering becomes prevalent when the concentration of $LaAsO_4:Eu^{3+}$ exceeds 14%, which results in lower lumen output. As such, Figure 8 demonstrates that the lumen first displays a noticeable rise, achieves its peak and subsequently displays a minor fall. Figures 8(a) to (b) demonstrates the considerable DRPS brilliance decrease as the red emitting phosphorus $LaAsO_4:Eu^{3+}$ concentration rises. This is caused by the considerable decrease in the light transmission energy via the red emitting phosphorus film. At all ACCTs, on the other hand, using 2-14% $LaAsO_4:Eu^{3+}$ the lumen output of DRPS is indeed considerably higher compared to that of SRPS. This proves that, beside CQS, the DRPS structure yields a greater brightness for WLEDs than SRPS.

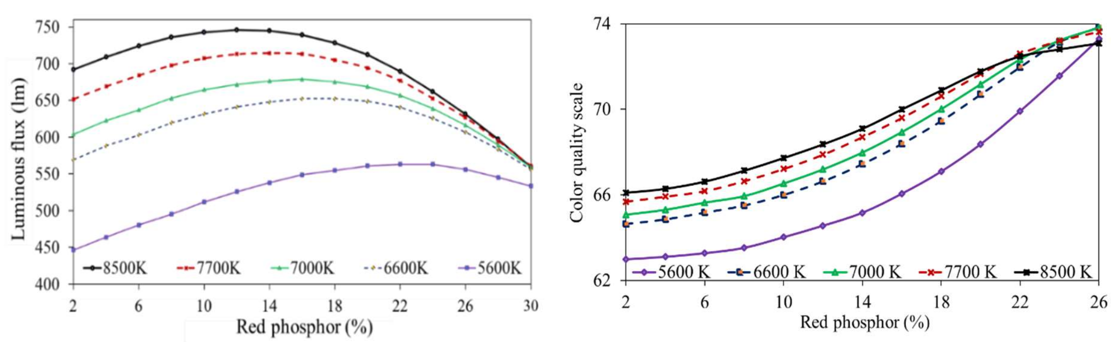


(a) (b)

Figure 8. SRPS luminous emissions featuring $LaAsO_4:Eu^{3+}$ (a) concentration and (b) DRPS

## 5. CONCLUSION

This research has focused on solving two issues: the first is comparing CQS and LED of the two structures SRPS and DRPS, the second is analyzing the influence of the red phosphor $LaAsO_4:Eu^{3+}$ upon both configurations' CQS and luminosity (LF) value. To achieve optimum CQS and LE, characteristics of phosphor pattern and concentration must be determined at the same time. The outcomes leading to the CRI and CQS increase as the $LaAsO_4:Eu^{3+}$ concentration increases. CQS can reach 74 when DRPS is employed ay ACCTs 5600 K–8500 K, while LF decreases considerably in contrast. However, at all ACCTs, the DRPS lumen output is constantly considerably higher in comparison with SRPS lumen output at 2-14% $LaAsO_4:Eu^{3+}$. In order to clarify such result, the scattering properties of $LaAsO_4:Eu^{3+}$, which includes the scattered coefficients $\mu_{sca}(\lambda)$, anisotropy element $g(\lambda)$, decreased scattered coefficients $\delta_{sca}(\lambda)$, and the angular scattered amplitudes $S_1(\theta)$ and $S_2(\theta)$ are also presented. To conclude, in term of the CQS and LF, DRPS is superior to SRPS, while the both configurations CRI values are nearly identical. To obtain optimum CQS and LF, the $LaAsO_4:Eu^{3+}$ concentration should be carefully determined.

## REFERENCES


[1] N. S. Zailani, M. F. Ghazli, R. Hussin, S. Z. Abd. Rahim, and M. N. Mat Saad, "Effects of Sm3+ on Luminescent Properties of LiEu(0.55-x)Y0.45 (WO4)2Smx Red Phosphor," *IOP Conf. Ser.: Mater. Sci. Eng*., vol. 374, no. 1, Jun. 2018, doi: 10.1088/1757-899X/374/1/012001.

[2] L. T. Ha, *et al*., "Effect of doping concentration and sintering temperature on structure and photoluminescence properties of blue/red emitting bi-phase Eu3+/Eu2+-doped Sr5(PO4)3Cl/Sr3(PO4)2 phosphors," *Mater. Res. Express*, vol. 5, no. 7, Jun. 2018, doi: 10.1088/2053-1591/aacf3b.

[3] L. Yang, G. Jiang, D. Wu and H. Chen, "Preparation of a Novel Red Y2MoSiO8: Eu3+, Dy3+ Phosphor," *IOP Conf. Ser.: Earth Environ. Sci*., vol. 714, no. 3, Mar. 2021, doi: 10.1088/1755-1315/714/3/032002.

[4] J. Xie and X. Zhang., "Synthesis and photoluminescence properties of ultraviolet excited Ba2MgWO6:Sm3+ orange-red phosphors," *IOP Conf. Ser.: Earth Environ. Sci*., vol. 639, no. 1, Jan. 2021, doi: 10.1088/1755-1315/639/1/012030.

[5] S. Adachi, "Photoluminescence Spectroscopy and Crystal-Field Parameters of Cr3+ Ion in Red and Deep Red-Emitting Phosphors," *ECS J. Solid State Sci. Technol.*, vol. 8, no. 12, Jan. 2019, doi: 10.1149/2.0061912jss.

[6] S. Cui, and G. Chen, "Investigation of photoluminescence properties, quenching mechanism and thermal stability of the red-emitting phosphor based on Eu ions doped apatite host NaLa9(SiO4)6O2,", *Mater. Res. Express*, vol. 6, no. 9, Jul. 2019, doi: 10.1088/2053-1591/ab2cfa.

[7] Y. Wang, Y. Wang, M. Wang, Y. Shao and Y. Zhu, "Facile preparation and formation mechanism of Sr2Si5N8:Eu2+ red-emitting phosphors," *Mater. Res. Express*, vol. 5, no. 5, May. 2018, doi: 10.1088/2053-1591/aabf82.

[8] X. Pan, D. Hou, M. Zhou, H. Lai, H. Ming and X. Ye., "HF-Free Preparation, High Thermal and Color Stability of Mn4+ Activated K2TiF6 Red Phosphors for White Light-Emitting Diodes," *ECS J. Solid State Sci. Technol*., vol. 7, no. 1, pp. R3006-R3011, 2018, doi: 10.1149/2.0011801jss.

[9] J. Silver, P. J. Marsh, G. R. Fern, T. G. Ireland and A. Salimian, "ZnCdS:Cu,Al,Cl: A Near Infra-Red Emissive Family of Phosphors for Marking, Coding, and Identification," *ECS J. Solid State Sci. Technol*., vol. 7, no. 1, pp. R3057-R3063, 2018, doi: 10.1149/2.0131801jss.

[10] X. Ma, S. Sun and J. Ma, "A novel orange-red Sr9Ga(PO4)7: Sm3+ phosphors for white light emitting diodes," *Mater. Res. Express*, vol. 6, no. 11, Oct. 2019, doi: 10.1088/2053-1591/ab47c6.

[11] X. Zhang, R. Cui, J. Zhang, X. Qi and C. Deng, "A Novel Red-Emitting Phosphor Ca2GdNbO6: Eu3+: Influences of Sintering Temperature and Eu3+ Concentration on the Photoluminescence," *ECS J. Solid State Sci. Technol*., vol. 10, no. 2, Feb. 2021, doi: 10.1149/2162-8777/abe1d7.

[12] K. Su, Q. Zhang, X. Yang and B. Ma, "Crystal structure and luminescence properties of thermally stable Sm3+-doped Sr9In(PO4)7 orange-red phosphor," *J. Phys. D: Appl. Phys*., vol. 53, no. 38, Jun. 2020, doi: 10.1088/1361-6463/ab938d.

[13] Y. V. Baklanova, L. G. Maksimova, O. A. Lipina, A. P. Tyutyunnik, A.Y. Chufarov and V. G. Zubkov., "A red-emitting phosphor based on Eu3+-doped Li6SrLa2Ta2O12 garnets for solid state lighting applications," *Mater. Res. Express*, vol. 6, no. 6, Mar. 2019, doi: 10.1088/2053-1591/ab093b.

[14] G. Rahate, V. R. Panse, S. J. Dhoble, N. S. Kokode and K. Sharma, "Photoluminescence studies and synthesis of KSrPO4:Ce3+, Eu3+ blue and orange-red emitting phosphor," *IOP Conf. Ser.: Mater. Sci. Eng*., vol. 1120, no. 1, pp. 1-9, 2021, doi: 10.1088/1757-899X/1120/1/012005.

[15] S. Adachi, "Review—Tanabe−Sugano Energy-Level Diagram and Racah Parameters in Mn4+-Activated Red and Deep Red-Emitting Phosphors," *ECS J. Solid State Sci. Technol*., vol. 8, no. 12, Dec. 2019, doi: 10.1149/2.0281912jss.

[16] L. Lei, Z. He, Z. Qun, Y. Chun-Feng, G. Chao-Chao and Y. Li, "Influences of sol-gel progress on luminescent properties of Li1.0Nb0.6Ti0.5O3:Eu3+ red phosphor," *Mater. Res. Express*, vol. 6, no. 4, Jan. 2019, doi: 10.1088/2053-1591/aaf91a.

[17] C. He, *et al*., "Preparation and photoluminescence properties of red-emitting phosphor ZnAl2O4:Eu3+ with an intense 5D0→7F2 transition," *Mater. Res. Express*, vol. 5, no. 5, 2018, doi: 10.1088/2053-1591/aaa7c9.

[18] O. M. ten Kate, Y. Zhao, K. M. B. Jansen, J. R. van Ommen and H. T. Hintzen, "Effects of Surface Modification on Optical Properties and Thermal Stability of K2SiF6:Mn4+ Red Phosphors by Deposition of an Ultrathin Al2O3 Layer Using Gas-Phase Deposition in a Fluidized Bed Reactor," *ECS J. Solid State Sci. Technol*., vol. 8, no. 6, Jun. 2019, doi: 10.1149/2.0281906jss.

[19] X. Yao, *et al*., "Preparation and Properties of Cr3+ Doped Mg0.388Al2.408O4 Red Phosphor," *IOP Conf. Ser.: Mater. Sci. Eng.*, 2020, pp. 1-5, doi: 10.1088/1757-899X/782/2/022020.

[20] Q. Wei, Z. Yang, Z. Yang, Q. Zhou and Z. Wang, "Communication—Luminescent Properties of Mn4+-Activated K3HfF7 Red Phosphor," *ECS J. Solid State Sci. Technol*., vol. 7, no. 5, Apr. 2018, doi: 10.1149/2.0051805jss.

[21] T. Pang and Z. Huang, "A novel upconverison phosphor Gd2Mo4O15:Yb3+, Ho3+: intense red emission and ratiometric temperature sensing under 980 nm excitation," *Mater. Res. Express*, vol. 5, no. 6, Jun. 2018, doi: 10.1088/2053-1591/aacc8e.

[22] Q. Wei, Z. Yang, Y. Liu, Q. Zhou and Z. Wang, "Communication—Highly Efficient Red-Emitting Phosphor Na2SiF6:Mn4+ Prepared in H3PO4 Environment," *ECS J. Solid State Sci. Technol*., vol. 9, no. 2, Feb. 2020, doi: 10.1149/2162-8777/ab709b.

[23] D. Shi *et al*., "Communication—Luminescence Properties of a Novel l Rb2KGaF6:Mn4+ Red-Emitting Phosphor for Solid-State Lighting," *ECS J. Solid State Sci. Technol*., vol. 9, no. 12, 2020, doi: 10.1149/2162-8777/abc835.

[24] N. Dhananjaya, S. R. Yashodha and C. Shivakumara, "The orange red luminescence and conductivity response of Eu3+ doped GdOF phosphor: synthesis, characterization and their Judd-Ofelt analysis," *Mater. Res. Express*, vol. 6, no. 12, 2019, doi: 10.1088/2053-1591/ab4a6b.

[25] Y. Masubuchi *et al*., "Large red-shift of luminescence from BaCN2:Eu2+ red phosphor under high pressure," *Appl. Phys. Express*, vol. 13, no. 4, 2020, doi: 10.1088/2053-1591/ab4a6b.

[26] T. G. Lim, Y. N. Ahm, H. W. Park and J. S. Yoo, "Red-Shifted Absorption of a Mn4+-Doped Germanate Phosphor by Crystal Distortion," *ECS J. Solid State Sci. Technol*., vol. 7, no. 1, pp. R3189-R3193, 2018, doi: 10.1149/2.0241801jss.

## BIOGRAPHIES OF AUTHORS

**Phuc Dang Huu** received a Physics Ph.D degree from the University of Science, Ho Chi Minh City, in 2018. Currently, He is Research Institute of Applied Technology, Thu Dau Mot University, Binh Duong Province, Vietnam. His research interests include simulation LEDs material, renewable energy. He can be contacted at email: danghuuphuc@tdmu.edu.vn.

**Dieu An Nguyen Thi** received a master of Electrical Engineering, HCMC University of Technology and Education, VietNam. Currently, she is a lecturer at the Faculty of Electrical Engineering Technology, Industrial University of Ho Chi Minh City, Vietnam. Her research interests are Theoretical Physics and Mathematical Physics. She can be contacted at email: nguyenthidieuan@iuh.edu.vn.